

Evolution of the UV Excess In Early-Type Galaxies

David W. Atlee, Roberto J. Assef and Christopher S. Kochanek¹

Department of Astronomy, The Ohio State University

atlee@astronomy.ohio-state.edu

ABSTRACT

We examine the UV emission from luminous early-type galaxies as a function of redshift. We perform a stacking analysis using Galaxy Evolution Explorer (GALEX) images of galaxies in the NOAO Deep Wide Field Survey (NDWFS) Boötes field and examine the evolution in the UV colors of the average galaxy. Our sample, selected to have minimal ongoing star formation based on the optical to mid-IR SEDs of the galaxies, includes 1843 galaxies spanning the redshift range $0.05 \leq z \leq 0.65$. We find evidence that the strength of the UV excess decreases, on average, with redshift, and our measurements also show moderate disagreement with previous models of the UV excess. Our results show little evolution in the shape of the UV continuum with redshift, consistent either with the binary model for the formation of Extreme Horizontal Branch (EHB) stars or with no evolution in EHB morphology with look-back time. However, the binary formation model predicts that the strength of the UV excess should also be relatively constant, in contradiction with our measured results. Finally, we see no significant influence of a galaxy's environment on the strength of its UV excess.

Subject headings: galaxies: evolution, ultraviolet: galaxies

1. Introduction

The UV excess is defined as the presence of more UV flux than predicted for a simple, old stellar population and was first reported by Code & Welch (1979). It is sometimes also called the UV upturn, because F_λ is seen to rise shortward of 2500\AA (Brown 2004). Donas, Milliard & Laget (1995), for example, found that the average early-type galaxy in

¹Center for Cosmology and Astroparticle Physics, The Ohio State University

the Coma cluster is more than a magnitude bluer in $m_{UV} - B$ than predicted by the population synthesis models of Bruzual & Charlot (1993). They explained the observed emission by invoking residual star formation (RSF), but it is unlikely that all of the early-type galaxies in the cluster experienced a recent burst of star formation at around the same time; this indicates the need for a source of UV emission not associated with star formation. Population synthesis models have since suggested a number of potential sources for this emission, usually involving significant mass loss by stars leaving the main sequence. The proposed sources include post-red giant stars, hot horizontal branch stars and post-AGB stars (e.g. Bressan et al. 1994). A combination of population synthesis models and high resolution spectra obtained with the Far UV Spectroscopic Explorer (FUSE; Brown et al. 2002) and the Hopkins Ultraviolet Telescope (HUT; e.g. Ferguson & Davidsen 1993) suggest that extreme horizontal branch (EHB) stars, also called hot subdwarfs (sdB), are the objects most likely to give rise to the UV emission, as the observed spectra closely match predictions from a population of EHB stars with various surface temperatures (Brown 2004).

Thus, conventional wisdom indicates that the stars giving rise to the UV emission are produced by significant mass loss from stellar envelopes on the red giant branch (RGB). If EHB stars are formed from stars with massive winds on the RGB, then the fraction of stars that find themselves in this unusual stage of stellar evolution, and thus the strength of the UV excess, should depend on the average metallicity of the host galaxy. Evidence for this picture can be found from several sources. First is the direct correlation between the strength of the UV excess and the Lick Mg_2 spectral index, which measures a galaxy’s average metallicity (Burstein et al. 1988). Also in keeping with such a metallicity dependence is the correlation between the UV excess and the mass (luminosity) of a galaxy suggested by O’Connell (1999). However, this correlation has recently become controversial. For example, Rich et al. (2005) found no apparent correlation between the Mg_2 index and the UV excess in a sample of 172 early-type galaxies from the Sloan Digital Sky Survey (SDSS). By contrast, Donas et al. (2007) found a weak but significant correlation among elliptical ($-5.5 \leq T < -3.5$) galaxies, but they found no such correlation in lenticular ($-3.5 \leq T < -1.5$) galaxies. They attribute this difference to the presence of residual star formation in lenticulars.

Recently, Ree et al. (2007; R07) used Galaxy Evolution Explorer (GALEX) photometry of galaxy clusters below redshift $z = 0.2$ to measure the evolution in the UV excess of Brightest Cluster Galaxies (BCGs) of rich clusters with redshift. The galaxies they measured showed no significant evolution, but by expanding their galaxy sample with objects studied using HST by Brown et al. (2000, 2003), they found that the $FUV - V$ colors of early-type galaxies in massive clusters become redder at higher redshift. They compare their expanded sample to two evolutionary models, one favoring sdB formation in metal-rich populations and the other favoring metal-poor populations, attempting to determine which model agrees

better with the measured colors. These models are developed by picking a pair of populations to bracket the $z = 0$ galaxies and then passively “evolving” them backwards in time. They find that both models agree reasonably well with the measurements, and marginally favor the metal-poor model.

Han, Podsiadlowski & Lynas-Gray (2007; HPL) suggested that sdB stars might form primarily via close binary interactions rather than forming via wind-driven mass loss on the RGB. Stars in close binary systems may eject much of their hydrogen envelope after they evolve off the main sequence via angular momentum exchange between the envelope and the binary companion. Their model makes several specific predictions, including that the correlation of the UV excess with metallicity should be weak, as should the evolution of the strength and shape of the UV excess with redshift. The HPL model is rather appealing, as it can explain the limited strength of the metallicity correlation found in the SDSS galaxies (Rich et al. 2005) and the large fraction of Galactic field sdB stars found in binary systems compared to those found in Galactic globular clusters (Catelan 2007).

The alternative hypotheses for the formation of sdB stars can be tested by examining the evolution of the UV colors of early-type galaxies with redshift. In this work we measure the evolution of the average early type galaxy by stacking GALEX images of galaxies in the Boötes field of the NOAO Deep Wide Field Survey (NDWFS). The galaxies are selected based on their optical to mid-IR spectral energy distribution (SEDs), following Assef et al. (2008). We study the UV emission from elliptical galaxies out to $z = 0.65$, where the number of sample galaxies in each redshift bin begins to diminish and the risk of AGN contamination increases. In §2 we describe our galaxy selection procedures. We describe our stacking algorithm and the analysis of the resulting images in §3, refine our galaxy selection criteria in §4, and we examine the evolution of the UV excess in §5. Finally, in §6 we consider the consequences of our measurements for models of sdB formation.

2. Target Selection

The Boötes field of the NOAO Deep Wide Field Survey (NDWFS) covers approximately 9 deg^2 centered at $(14^{\text{h}}32^{\text{m}}, +34^{\circ}17')$. We used the optical (NDWFS, Jannuzi & Dey 1999; zBoötes, Cool 2007), near-IR (NDWFS; FLAMEX, Elston et al. 2006) and mid-IR (The IRAC Shallow Survey, Eisenhardt et al. 2004) photometry for objects in the field. The AGN and Galaxy Evolution Survey (AGES) redshift catalog has galaxy spectra complete to $I = 18.5$ and an extended sample with $18.5 < I \leq 20$ for objects in the Boötes field (Kochanek et al. in prep). The AGES catalog contains spectroscopic redshifts for approximately 17,000 objects, and we use these redshifts for the galaxies in our sample wherever

possible. We rely on photometric redshifts for objects without spectroscopy, which is the majority of our sample.

The GALEX satellite is conducting a survey of the ultraviolet sky in two photometric bands, the Far-UV (FUV ; $\lambda_{eff} = 1528\text{\AA}$, $\Delta\lambda = 442\text{\AA}$) and Near-UV (NUV ; $\lambda_{eff} = 2271\text{\AA}$, $\Delta\lambda = 1060\text{\AA}$; Morrissey et al. 2005). We acquired GALEX Release 3 (GR3) images of sixteen GALEX Deep Imaging Survey (DIS) fields overlap the Boötes field. The names and GR3 exposure times for all sixteen fields, in both the FUV and NUV bands, are listed in Table 1. The different pointings vary widely in depth for both the FUV and NUV bandpasses, with a typical integration time for the NUV fields of approximately 7000s. The FUV pointings are fewer and their exposure times more widely distributed.

Assef et al. (2008) developed and tested a set of three moderate-resolution template galaxy spectra extending from 0.2 to $10\mu\text{m}$. We used these templates to model the SEDs of the galaxies in the Boötes field with $I < 21.5$ mag by fitting the measured optical, NIR and MIR fluxes. The templates are able to distinguish between passively evolving galaxies and galaxies with on-going star formation based on their MIR fluxes, which are extremely sensitive to the PAH emission features associated with star formation. The MIR fluxes are also sensitive to the presence of AGN since the power-law continuum typical of AGN results in much stronger $3.6 - 4.5\mu\text{m}$ emission than is typical for a stellar population (Stern et al. 2007).

Using the template spectra, we identified passively evolving galaxies, eliminated AGN, computed K-corrections and synthesized unmeasured bands. We eliminated AGN from our galaxy sample by first removing any object flagged as an AGN or candidate AGN by AGES and accepting the remaining galaxies only if their photometry fit the galaxy templates with $\chi^2_\nu \leq 2.0$. AGES targeted galaxies as AGN candidates if they were identified as X-ray sources in the xBoötes survey (Murray et al. 2005), as radio sources by FIRST (Becker, White & Helfand 1995) or by de Vries et al. (2002), or as possessing a red mid-IR color (Stern et al. 2007). The AGES database further identifies galaxies as AGN by the spectral template used for estimating redshifts in a modified version of the Sloan Digital Sky Survey spectroscopic pipeline. Our χ^2_ν cut would eliminate the objects flagged based on their optical and MIR colors, but it is also able to identify AGN based solely on how well the measured fluxes agree with a purely stellar origin across a wide wavelength baseline (i.e. whether the B_w and IRAC $8\mu\text{m}$ fluxes can simultaneously agree with the I -band fluxes).

Assef et al. (2008) classified galaxies by the fraction of their bolometric luminosity contributed by the elliptical component of their SED, designated \hat{e} . We selected an initial sample of early-type galaxies by requiring $\hat{e} \geq 0.8$, which Assef et al. (2008) found roughly divides the Red Sequence the Blue Clump for galaxies in the Boötes field. We also required that

galaxies in our sample have “bolometric” luminosities, computed using the model SEDs, in the range $0.5 \leq \log\left(\frac{L_{\text{bol}}}{10^{10}L_{\odot}}\right) \leq 1.5$. This roughly corresponds to $-24 \leq M_R \leq -21.5$. After applying these selection criteria, we eliminated an additional seven galaxies whose MIR fluxes exceed their K_s fluxes, since these galaxies may host hidden AGN or are otherwise unusual. These criteria yield an initial sample of 6630 galaxies in the range $0 \leq z \leq 0.65$.

3. Galaxy Stacking

We divided our galaxy sample into redshift bins of width $\Delta z = 0.1$, using spectroscopic redshifts from AGES where available and photometric redshifts from fits to the Assef et al. (2008) spectral templates otherwise (approximately 80% of the initial sample). The photo-z algorithm we employ has been extensively discussed in Assef et al. (2008). For early-type galaxies, it is accurate to $\Delta z/z \approx 0.02$ based on comparisons to AGES spectroscopic redshifts (see their Fig. 9).

Of the 6630 galaxies with $\hat{e} > 0.80$, 328 (122) were detected as individual GALEX sources in the $NUV(FUV)$ and appear in the GALEX catalogs; the majority of these belong to the first two redshift bins. Since the vast majority of galaxies in the sample had no measured UV fluxes, we employed a stacking analysis to measure the exposure-weighted mean UV fluxes of our galaxy sample as a function of redshift. One obvious disadvantage of this approach is that we are insensitive to variations in individual galaxy properties. For example, we will be unable to measure the presence or strength of any correlation between the UV excess and metallicity.

We stack the GALEX images of the Boötes field, as described in §3.1, to measure the average UV fluxes of our sample galaxies. We also require optical fluxes to compare with the UV emission. We obtain these by computing exposure-weighted averages of the measured optical, NIR and MIR fluxes for the galaxies in our sample. Since the Boötes photometry is much deeper than the GALEX pointings, the statistical errors on the appropriately averaged optical fluxes are much smaller than the uncertainty on the stacked GALEX magnitudes; in fact, the systematic uncertainties associated with the Boötes photometry dominate the error budget of the optical, NIR and MIR photometry. In order to account for the systematic uncertainties, we assign the averaged magnitudes an uncertainty of 0.05 magnitudes before fitting to the spectral templates (see §3.2) unless the statistical uncertainty implied by averaging the fluxes exceeds this value. The statistical uncertainties only exceeded this systematic limit in the case of the K_s band observations, for which a small number of galaxies with exceptionally large uncertainties dominate the error budget.

3.1. GALEX Image Stacking

We obtained the GALEX observations for each DIS field as well as the associated source catalogs from the GALEX archive at the Space Telescope Science Institute¹. The pixel scale of these images is 1".5 per pixel. We use the *Funtools*² package to parse the images and manage the stacking. We masked identified GALEX sources falling outside an annulus with diameter equal to twice the FWHM of the PSF and centered on the nearest target galaxy; this guaranteed that the stacked images had a well-defined sky flux. It also means that we masked differently in the *FUV* and *NUV* images, both because the PSF size differs between the two bands (4".5 and 6".0 in the *FUV* and *NUV*, respectively) and because there are more sources in the *NUV*. We extracted a list of identified sources from the GALEX catalog for comparison with the sample galaxies belonging to each redshift bin. We identified a set of GALEX objects to be masked by comparing the central coordinates of the objects in the two lists and created separate masked images for each redshift bin.

Once we identified a GALEX source to be masked, we examined a series of square frames expanding outward from the center listed in the catalog, determining whether each individual pixel in the frame needed to be masked. We masked pixels whose fluxes exceeded the sky background by more than 1σ and all those within the FWHM of the PSF. If more than half of the pixels in a given frame were masked, we expanded the masking region by one pixel in each direction and processed the next frame. In all cases we terminated the process if the masking region reached 50 pixels from the center. The flux in masked pixels was set to the nominal sky flux in the appropriate band (Morrissey et al. 2005). We deliberately allowed the masking of flagged objects to extend over nearby objects, as this limited the contamination of the stacked images by stray flux from nearby objects. It also removed some flux from the target galaxies, which can introduce a bias. We tested the algorithm and found the effects of this bias to be small (§3.3). A visual comparison of the GALEX images before and after masking indicated that the masking algorithm was quite efficient.

After converting the masked images from counts s^{-1} to counts, we added the counts in an 81×81 pixel ($121".5 \times 121".5$) box around each galaxy in a given redshift bin. We divided the number of counts in each stacked pixel by the total exposure time, converting the counts back to counts s^{-1} . The masking and stacking procedures were repeated for each of six redshift bins, centered from $z = 0.1$ to $z = 0.6$. Our stacked galaxy images from each redshift bin are shown in Figure 1. All of the stacked images beyond the $z = 0.1$ redshift bin

¹<http://galex.stsci.edu/GR2/?page=tilelist&survey=dis>

²<http://hea-www.harvard.edu/saord/funtools/>

are consistent with the contributing objects being unresolved, as expected for the angular resolution of GALEX.

The choices we made in setting the parameters of our masking algorithm were very conservative, especially the decision to mask pixels down to 1σ above the mean sky level. These choices were necessitated by the very large number of galaxies, often several hundred, that go into a single stacked image. In order to insure that we measure the sky flux correctly and that we do not introduce stray flux from the outskirts of nearby sources into the stacked galaxies, we require our masking algorithm to err on the side of caution. This decision makes it easier to address any intrinsic contamination in our sample.

3.2. UV Photometry

We performed our UV photometry using the IRAF *phot* program with $15''$ diameter photometric apertures. We converted the measured count rates to magnitudes using the GALEX photometric zero points (Morrissey et al. 2005):

$$m_{FUV} = \log(f_{FUV}) + 18.82 \quad (1)$$

$$m_{NUV} = \log(f_{NUV}) + 20.08 \quad (2)$$

where f_X is the count rate in band X . We also obtained optical, NIR and MIR fluxes in the same aperture from the NDWFS, FLAMEX and IRAC Shallow surveys where available.

Our large photometric aperture is required by the irregularity of the GALEX PSF, which differs between bands and depends on the position of a source in the image (Martin et al. 2005). Using a Moffat PSF profile with $\beta = 3$, which is a reasonable match to the GALEX PSF, we computed aperture corrections for our FUV and NUV magnitudes. Our targets were effectively point sources beyond $z = 0.1$, so a $15''$ aperture includes 99% and 97% of the FUV and NUV fluxes, respectively. These translate to aperture corrections of 0.01 and 0.02 magnitudes for the FUV and NUV bands, respectively. Both corrections are significantly smaller than the errors in the mean stacked magnitudes, so we neglect them.

We computed Galactic extinction corrections using the polynomial extinction law of Cardelli, Clayton & Mathis (1989) based on the mean $E(B - V)$ of 0.011 for objects in the Boötes field (Schlegel, Finkbeiner & Davis 1998). Due to the rapid changes in extinction across the GALEX photometric bands, we computed a weighted average of the R_λ values across each GALEX bandpass,

$$R_x = \frac{\int_{\lambda_1}^{\lambda_2} R(\lambda)T(\lambda)d\lambda}{\int_{\lambda_1}^{\lambda_2} T(\lambda)d\lambda}, \quad (3)$$

where $R(\lambda)$ is the Cardelli, Clayton & Mathis (1989) R-value at wavelength λ , $T(\lambda)$ is the filter bandpass, and the extinction in band X is given by $A_x = R_x \times E(B - V)$. Using Eq. (3), we found $R_{FUV} = 8.24$ and $R_{NUV} = 8.10$.

We used bootstrap re-sampling of our galaxies to estimate the uncertainty on the mean magnitude. This procedure naturally includes both counting statistics and the effects of intrinsic scatter in the sample population, which could easily cause the uncertainty in the mean magnitude to exceed the intrinsic photometric uncertainty. Any factor that leads to variation in L_{UV} at fixed L_{bol} might contribute to the measured scatter. Such variables include metallicity (Burstein et al. 1988), age (Bressan et al. 1994), recent star formation (Kaviraj et al. 2007) and total stellar mass (O’Connell 1999). Our bootstrapping analysis folds all such intrinsic variations in our galaxy sample into the error on the mean magnitude. We drew 250 bootstrapping realizations in each redshift bin and used the RMS of the resulting magnitudes as the uncertainty on the mean magnitude. The results of these calculations are listed in Table 2.

We did not use the Assef et al. (2008) spectral templates in our final analysis because they were computed without using UV photometry to constrain the shapes of the spectral templates beyond $\lambda \approx 3000\text{\AA}$. Instead, we rely on new, unpublished templates (Assef et al. in prep) that have been modified by employing GALEX photometry and MIPS $24\mu m$ fluxes to provide additional constraints on the shapes of the templates. These templates were developed using the techniques described in Assef et al. (2008) and employing the additional UV and MIR photometry. The new templates significantly improve the quality of the fit to our stacked UV data, and we therefore rely on them for UV K-corrections. The new elliptical template is compared with the published version in Figure 2. The figure also shows the spiral and (new) AGN templates for comparison. It is apparent that the contributions of AGN and star-formation can be significant, and it is important that we eliminate these contaminants wherever possible and subtract the contribution to the measured UV fluxes where they cannot be eliminated. (See §5.)

3.3. Stacking Tests

We conducted two tests to verify that our stacking code behaved as expected. First, we tested whether the masking algorithm affected the measured fluxes from the the stacked galaxies, whether by removing flux from the target galaxies or by adding extra flux through poor masking of nearby sources. We divided the 122 galaxies with identified GALEX counterparts in both the FUV and NUV into redshift bins and stacked them. We compared the magnitudes of our stacked images with the magnitudes predicted using the fluxes in the

GALEX catalog. The results, listed in Table 2, suggest a small bias of approximately 0.05 mag, which is similar to the typical uncertainty on the bias. Also included in Table 2 are the dispersions about the mean magnitude and the estimated bias, showing that any bias in the measured fluxes is small compared to the intrinsic scatter in the measured fluxes.

We also repeated our entire analysis chain on a set of ~ 8000 galaxies selected to be strongly star-forming—galaxies with an elliptical contribution to their bolometric luminosity of less than 20%. We compared the colors of the stacked star-forming galaxies to those of passively evolving galaxies, as shown in Figure 3. (Figure 3 was created using the photometry of the final galaxy sample, as discussed in §4, and uses V magnitudes computed using the template SEDs.) We compute the uncertainties on our colors using the bootstrap uncertainties for the FUV magnitudes and setting $\sigma_V = \sqrt{[(Bw - Bw_{\text{model}})^2 + (R - R_{\text{model}})^2]}/2$. As expected, the average star forming galaxy was significantly bluer than the average elliptical galaxy. Furthermore, the colors of the stacked galaxies agree well with the colors of the template spectra at low redshifts and show different evolution in their $FUV - V$ colors compared to the early-type sample. This indicates that our stacking procedure does not introduce a bias toward bluer $FUV - V$ color at high redshift. This is significant because, as apparent from Figure 3, the $FUV - V$ colors of our stacked galaxies become somewhat bluer with increasing redshift.

4. Refining the Galaxy Sample

We selected our initial sample based on the results of Assef et al. (2008), who found that galaxies with $\hat{e} \geq 0.80$ fall on the red sequence. However, the UV photometry we used is more sensitive to low levels of star formation than optical photometry (e.g. Kaviraj et al. 2007), and we needed to determine whether any of our selection criteria introduce an obvious bias in our galaxy sample. We therefore broke our galaxies into subsamples according to various properties and looked for any significant differences between them.

We examined the effect of our three selection criteria— \hat{e} , luminosity and the χ_ν^2 of the fit to the template spectra—on the redshift evolution of the observed $FUV - V$ color of the stacked galaxies, which is an indicator for the strength of the UV excess. The results are shown in Figure 4. There is no significant bias associated with χ_ν^2 . While a small trend with luminosity is observed, it is only marginally significant. Also, the sense of the trend is to introduce a systematic shift toward redder $FUV - V$ at all redshifts. This does not affect the observed global trend, and is therefore little cause for concern. However, it should be noted that a sample with different $\langle L_{\text{bol}} \rangle$ will show slightly different colors. Examining the variation in $FUV - V$ between samples binned in stellar mass would not yield additional

information because we have selected only early-type galaxies, so there will be little variation in mass-to-light ratio.

The \hat{e} test suggests that the initial $\hat{e} > 0.80$ limit is too loose. For the rest of our analysis, we used a stricter $\hat{e} > 0.925$ limit to reduce the contribution of recent star formation as much as possible. We compared the results using this criterion to those obtained using $\hat{e} > 0.87$. The new $\hat{e} > 0.925$ ($\hat{e} > 0.87$) limit left 1843 (4943) of the original 6330 galaxies. The uncertainties in our optical and IR photometry are still dominated by systematic issues in both cases. Figure 5 shows the distribution of galaxies in \hat{e} as a function of redshift. The distribution broadens toward higher redshift largely because the redshift of the PAH emission features (see Fig. 2) reduces our ability to detect low-level star formation. Some of the increase in the fraction of low- \hat{e} galaxies is due to evolution in the stellar populations of the sample galaxies. Note that the peak in the \hat{e} -distribution only moves by $\Delta\hat{e} \approx 0.03$ between panels. A strict \hat{e} limit reduces the contribution from both of these effects, but it cannot eliminate them. As a result, Figure 6 shows an increased contribution from the Sab template at higher redshift.

The magnitudes we measured from our stacked images are listed in Table 3 along with the associated errors and K-corrections. We examined the evolution of $\langle\hat{e}\rangle$ with redshift and found no significant trend in either the $\hat{e} \geq 0.925$ or $\hat{e} \geq 0.87$ cases. We verified that the choice between the two alternative selection criteria has little effect on our conclusions by comparing the results obtained using the two \hat{e} selection criteria, which effectively correspond to two different rest-frame color cuts. We could adopt an \hat{e} limit that varies with redshift to allow for evolution in the optical properties of early-type galaxies, but we choose not to do so because it would also lead to changes in our sensitivity to star formation and low-level AGN contamination.

We also stacked the AGES spectra of the galaxies in bins of \hat{e} to determine how significantly contamination by star formation or low-level nuclear activity may contribute to our results. We divided the sample into three different \hat{e} bins and examined the spectra in the vicinity of the [OII] 3727Å, [OIII]4959,5007Å and H α emission lines. The stacked spectra are shown in Figure 7 and indicate the presence of very weak LINERs, which we could not have detected in a typical individual spectrum. The agreement between the mean and median spectra indicates that the features are common to most of the galaxies in our sample rather than being restricted to a few unusual objects. The strength of the features also decreases with increasing \hat{e} , further motivating the use of the stricter $\hat{e} > 0.925$ limit. We have now exhausted our ability to reduce the presence of weak AGN, and we must consider this minimal contamination in the interpretation of our results.

One additional source of contamination that might be important, especially at higher

redshifts, is blending of the UV light in galaxies with nearby star-forming companions due to the large scale of the GALEX PSF. To assess this possibility, we searched the optical catalogs for objects within $4''.5$ ($6''.0$) of our $\hat{e} \geq 0.925$ sample and with $I \leq 22.5$; beyond these radii, any object with a significant UV flux would have been masked. We found 43 (226) total matches to the 1843 objects in the sample. If we fit the photometry of the companions with the Assef et al. (in prep) templates, compute their rest-frame colors and require that any “contaminating” companions have $B - R$ at least 0.1 mag bluer than a pure elliptical, only 8 (42) companions survive. We eliminated those galaxies with a blue companion and repeated our analysis. The resulting UV fluxes were consistent with the main sample given the uncertainties.

5. Redshift Evolution

In Figure 6, we show the average spectral energy densities of the stacked $\hat{e} > 0.925$ galaxies as a function of redshift, including the average optical, near-IR and mid-IR fluxes of the sources. It is apparent that the templates provide adequate fits in all redshift bins out to $z = 0.4$, but the last two redshift bins show discrepancies. The fit to the UV fluxes in the $z = 0.6$ bin is particularly bad because increasing the late-type contribution to fit the UV fluxes would overpredict the MIR fluxes, which have smaller uncertainties. This may be due, in part, to evolution in the shape of the UV excess with look-back time (e.g. Brown et al. 2000). Early-type galaxies are also known to grow bluer and brighter with increasing redshift due to their younger stellar populations (e.g. Ferreras et al. 2005), which the templates model by changing the relative contributions of the various components. Changes in the intrinsic shape of the stellar SEDs may lead to under-predicting the UV flux of a passively-evolving stellar population. We see some evidence for this in Figure 5, in which the \hat{e} -distribution moves to lower \hat{e} with redshift out to $z = 0.4$, and in Figure 6, which shows an excess of both UV and MIR emission in the $z = 0.6$ bin.

Figure 3 shows the evolution of the measured $FUV - V$ colors (uncorrected for star formation) of our stacked galaxies. The $FUV - V$ color of the uncorrected galaxies becomes moderately bluer at higher redshifts, in contrast with the results of R07, which suggest that color stays relatively constant with redshift. The K-corrected colors, shown in the lower panel, indicate that the rest-frame colors exhibit no obvious evolution.

While the late-type templates never contribute a significant fraction of the bolometric luminosity, averaging only 7%, their contribution to the UV flux can be significant. The colors shown in Figure 3 do not account for contamination by star formation, so we must correct for the contribution of star formation to the measured UV fluxes before attempting

to interpret the colors in the context of the UV excess. If we assume that half of the UV flux in all redshift bins beyond $z = 0.2$ is contributed by star formation, then a correction of 0.75 magnitudes to the $FUV - V$ colors is required. Such a correction would bring our colors into rough agreement with the colors reported in R07. Since the results of Figure 7 indicate that \hat{e} is a reasonable tracer of contamination, we can use the templates to estimate the contribution of young stars to the measured UV flux. These young stars may be due to recent star formation or a component of the old stellar population that has not yet evolved off the main sequence. At any given wavelength, the two late-type templates contribute a fraction of the total flux, r_{sf} , given by

$$r_{sf}(\lambda) = \frac{f_{spiral}(\lambda) + f_{irregular}(\lambda)}{f_{ellip}(\lambda) + f_{spiral}(\lambda) + f_{irregular}(\lambda)} \quad (4)$$

where $f_x(\lambda)$ is the density from template x at wavelength λ . If we assume that the UV flux from the elliptical template has no contribution from young stars and that the UV fluxes from the two star forming templates are contributed entirely by young stars, we can then determine the $FUV - V$ colors the stacked galaxies would have in the absence of young stars,

$$(FUV - V)_{corr} = (FUV - V)_{obs} - 2.5 \log \left[1 - r_{sf}(1550\text{\AA}) \right] \quad (5)$$

where $r_{sf}(1550\text{\AA})$ is the fraction of flux contributed by star formation at the approximate center of the FUV band. The correction to the V -band magnitudes is negligible for the relevant values of \hat{e} . The corrections derived using this approach are not exact because the star forming templates will likely have at least a small contribution to their UV fluxes from hot, old stars and the elliptical template will similarly contain a contribution from low-level star formation.

If we use the corrected colors derived from Eq. (5), our results agree reasonably well with previous measurements, as shown in Figure 8. The resulting colors from both the $\hat{e} > 0.925$ and $\hat{e} > 0.87$ samples agree within the error bars, despite the different corrections for star formation, so we conclude that our approach is robust. This agreement also suggests that our use of a fixed \hat{e} cut to select our galaxy sample does not significantly bias our conclusions. While the Brown et al. (2003) colors show a slight disagreement with our results, the significant scatter about the mean colors can likely account for the observed differences. The $z = 0.6$ bin remains quite blue, probably because of the poor fit to the UV fluxes (see Fig. 6).

Figure 8 indicates a systematic disagreement between our high- z measurements and the non-evolving “model” for the UV excess. While the \hat{e} data points are discrepant at only the 1σ level, the considerably better statistics in the $\hat{e} > 0.87$ sample lead to disagreement at the 2σ level in each redshift bin. Disregarding the $z = 0.6$ bin due to its poor fit, there

is a 23% (0.6%) probability of getting 3/5 data points to disagree with the model at the $1\sigma(2\sigma)$ level. If we also disregard the $z = 0.5$ data point, these probabilities increase to 38% and 2%, respectively. This indicates that, while our highest quality sample is consistent with an unevolving model, the extended ($\hat{e} \geq 0.87$) sample is not. The two samples return basically the same results, so we can reject an unevolving model for the UV excess at $>98\%$ confidence.

In addition to considering the strength of the UV excess, we examine its intrinsic shape by looking at the $FUV - NUV$ colors of the stacked galaxies, as shown in Figure 9. Figure 9a shows that the modified templates provide a reasonable approximation to the shape of the UV excess over our entire redshift range. The agreement between the measured and predicted colors in the $z = 0.6$ bin indicates that the disagreement between the measured fluxes and the model spectrum in Figure 6 is one of normalization rather than shape. We have not corrected the colors in Figure 9 for star formation because any such correction will depend critically on the assumed shape of the UV excess, which we are trying to measure. Assuming that the early- and late-type templates give a reasonable match to the UV excess and the emission from young stars, respectively, the values of r_{sf} (1550) and r_{sf} (2250) should be similar and the correction small. (See Fig. 6.) Figure 9b compares our K-corrected UV colors to the prediction in HPL; the error bars in this panel do not include the systematic uncertainties associated with applying K-corrections from the model spectra. The colors in Figure 9b appear to show moderate evolution toward redder $FUV - NUV$ beyond $z = 0.4$, and are inconsistent with the HPL model. However, if we use the differences between the measured $FUV - NUV$ colors and those predicted by the templates to estimate the systematic uncertainties associated with the templates, the error bars on the $z = 0.5$ and $z = 0.6$ redshift bins increase by $\sim 75\%$, and we are no longer able to distinguish between the HPL model and an unevolving spectral shape.

The principle difference between our work and existing studies is that we examined a sample including all early-type galaxies above a fixed luminosity cutoff rather than restricting the sample to galaxies in rich clusters. Since galaxies in clusters are likely to be stripped of their gas, they are also less likely to show recent star formation. Different star formation histories may also affect the metallicity distributions of cluster ellipticals compared to those in the field, and either effect could alter the UV properties of galaxies in rich clusters.

We measure the effect of a galaxy’s environment on its UV properties by counting the number of bright elliptical galaxies within a projected radius of $2h^{-1}$ Mpc of each sample galaxy and within a photometric $\Delta z = 0.03$, which is similar to the resolution of our photometric redshifts. We sorted the galaxies in our $\hat{e} > 0.925$ sample in order of increasing numbers of nearby bright ellipticals and divided the sample into four bins labeled 1-4 (low

density to high density) with equal numbers of galaxies in each bin. We stacked the galaxies in each density bin as described in §3.1, and the results are shown in Figure 10. The displayed colors have not been corrected for residual star formation, but since the different samples have similar $\langle \hat{e} \rangle$, the corrections for the different density samples should also be similar. The trend toward bluer $FUV - V$ color at higher redshift is found in all density bins, although the scatter between the samples is sometimes significant. We do not find any significant trend in $FUV - V$ as a function of environment. This suggests that either the Horizontal Branch morphology does not differ significantly between clusters and the field or the galaxies that are significantly affected by their environment are so rare that the effects are overwhelmed by averaging with a large number of “normal” galaxies.

6. Summary and Conclusions

We have measured the evolution of the UV emission from the average luminous, early-type galaxy with redshift by performing a stacking analysis with photometrically selected galaxies from the Boötes field. To the extent possible with the available data, we have eliminated AGN from our sample, although the stacked AGES spectra suggest that weak LINERs are ubiquitous. LINERs show very weak UV continua compared to broad-line AGN of similar luminosity, so the contamination of our results due to nuclear activity is minimal. We find that the observed $FUV - V$ colors of our stacked galaxies are bluer than the colors of the BCGs studied by Ree et al. (2007), Brown et al. (2000) and Brown et al. (2003) and show a pronounced tendency to become bluer with redshift. The presence of a small excess in $8\mu m$ emission indicates the need to correct for residual star formation. The necessity of such a correction, even among a sample of galaxies that has been carefully selected to have as little star formation as possible, suggests that contributions from star formation should always be considered when measuring the UV excess photometrically. This is consistent with the results of other authors (e.g. Kaviraj et al. 2007).

After correcting for star formation, we find that the intrinsic strength of the UV excess, as measured by the $FUV - V$ colors, is inconsistent with a non-evolving model. The measured evolution shows reasonable agreement with previous studies. However, the $FUV - V$ colors of the averaged galaxies remain modestly bluer than the individual cluster galaxies that have been studied previously. Our results agree with the R07 results in the first two redshift bins, but their preferred models are inconsistent with our higher redshift data, suggesting that one or more of the model parameters needs to be adjusted. At least some of the evolution may be due to an increase in $\langle L_{bol} \rangle$ from $5 \times 10^{10} L_{\odot}$ to $8 \times 10^{10} L_{\odot}$ as we go from $z = 0.1$ to $z = 0.5$, since more luminous galaxies tend to show redder $FUV - V$. The relatively

good agreement between our results and the individual galaxies measured by other authors indicates that our stacking analysis is able to probe the evolution of the UV excess as well as detailed studies using small galaxy samples.

We also measured the evolution of the intrinsic shape of the UV excess, finding little evidence for evolution in the rest-frame $FUV - NUV$ colors of early-type galaxies in the 6 Gyr since $z = 0.6$. Our two highest-redshift data points are slightly redder than the others, possibly due to systematic effects in our K-corrections, but the differences are not significant. The UV colors of our stacked galaxies are also consistent with the slow evolution predicted by HPL, but the change in the intrinsic $FUV - V$ color with redshift is inconsistent with their predictions for the evolution in the UV-optical color. While HPL do not show any predictions for evolution in $FUV - V$, they do predict the change in $FUV - r$, which should be quite similar to $FUV - V$, to be only ~ 0.1 mag. (See HPL, Figure 3.)

We found evidence that the UV excess might weaken in more luminous, and therefore more massive, galaxies. The evidence for this trend is marginal at best, however, and this result should be explored further. If true, it would contradict the suggestion that the UV excess is stronger in more metal-rich galaxies, since the most massive galaxies tend also to have the highest metallicities.

We also divided our galaxies into subsamples by density to explore the impact of environment on the UV excess, and found that the trend for bluer $FUV - V$ colors at higher redshift occurs in all environments. There is no identifiable trend in color with density. The lack of such trends is surprising, as effects such as ram pressure stripping, felt by galaxies in rich clusters, could lead to changes in the age, mean metallicity or residual star formation rates of the constituent galaxies.

While several open questions remain, including the possible variation in the UV excess with stellar mass, it appears that the average early-type galaxy evolves in roughly the same way as the individual cluster galaxies measured thus far. The measured evolution, along with the lack of significant trends in color with galaxy environment, should provide interesting constraints for future models of stellar evolution.

We wish to thank Thomas Brown and Henry Ferguson for providing us with their published UV spectra for a sample of elliptical galaxies; while not used in the final text, these spectra were extremely useful for earlier versions of this work. We are grateful to Tim Heckman for answering occasional questions concerning the GALEX satellite and for helpful suggestions for ways to exclude possible instrumental effects as sources of systematic uncertainty. Thanks are due Marc Pinsonneault, Michael Brown, Daniel Stern, Anthony Gonzalez and an anonymous referee for their helpful comments on earlier drafts of this

paper. We thank Rick Pogge for a useful discussion concerning the our stacked spectra. Additionally, we wish to thank the developers of the Funtools package of FITS utilities, which we used extensively in our masking and stacking routines. We acknowledge the GALEX collaboration for providing access to the DIS images used in this work. This work made use of data products provided by the NOAO Deep Wide-Field Survey (Jannuzi and Dey 1999; Jannuzi et al. 2005; Dey et al. 2005), which is supported by the National Optical Astronomy Observatory (NOAO). NOAO is operated by AURA, Inc., under a cooperative agreement with the National Science Foundation.

REFERENCES

- Assef, R.J., et al. 2008, ApJ, 676, 286
- Assef, R.J. et al. *in preparation*
- Becker, R.H., White, R.L. & Helfand, D.J. 1995, ApJ, 450, 559
- Bianchi, L., et al. 1999, Mem. Soc. Astron. Ital., 70, 365
- Bressan, A., Chiosi, C., & Fagotto, F. 1994, ApJS, 94, 63
- Blanton, M.R., & Roweis, S. 2007, AJ, 133, 734
- Brown, T.M., Bowers, C.W., Kimble, R.A., Ferguson, H.C. 2000, ApJ, 529, L89
- Brown, T.M., Ferguson, H.C., O’Connell, R.W., Ohl, R.G. 2002, ApJ, 568, L19
- Brown, T.M., Ferguson, H.C., & Davidsen, A.F. 1995, ApJ, 454, L15
- Brown, T.M., Ferguson, H.C., Deharveng, J. & Jedrejewski, R.I. 1998, ApJ, 508, L139
- Brown, T.M., et al. 2003, ApJ, 584, L69
- Brown, T.M. 2004, Ap&SS, 291, 215
- Bruzual, G.A. & Charlot, S. 1993, ApJ, 405, 538
- Burstein, D., Bertola, F., Buson, L.M., Faber, S.M., Lauer, T.R. 1988, ApJ, 328, 440
- Cardelli, J.A., Clayton G.C., & Mathis, J.S. 1989, ApJ, 345, 245
- Catelan, M. 2007, arXiv: 0708.2445
- Code, A.D. & Welch, G.A. 1979, ApJ, 228, 95

- Cool, R.J. 2007, ApJS, 169, 21
- Donas, J., Milliard, B. & Laget, M. 1995, A&A, 303, 661
- Donas, J., et al. 2007, ApJS, 173, 597
- Elston, R.J., et al. 2006, ApJ, 639, 816
- Eisenhardt, P.R., et al. 2004, ApJS, 154, 48
- Eisenhardt, P.R., et al. 2007, ApJS, 169, 225
- Eisenstein, D.J. et al. 2003, ApJ, 585, 694
- Ferguson, H.C., et al. 1991, ApJ, 382, L69
- Ferguson, H.C. & Davidsen, A.F. 1993, ApJ, 408, 92
- Ferreras, I., Lisker, T., Carollo, C.M., Lilly, S.J., Mobasher, B. 2005, ApJ, 635, 243
- Han, Z., Podsiadlowski, Ph. & Lynas-Gray, A.E. 2007, MNRAS, 380, 1098
- Jannuzi, B.T. & Dey, A. 1999, ASP Conference Series, Vol 191, p. 111
- Kaviraj, S., et al. 2007, ApJS, 173, 619
- Kochanek, C.S., et al. *in preparation*
- Martin, D.C., et al. 2005, ApJ, 619, L1
- Morrissey, P., et al. 2005, ApJ, 619, L7
- Murray, S.S., et al. 2005, ApJS, 161, 1
- O’Connell, R.W. 1999, A&A, 37, 603
- Ree, C.H., et al. 2007, ApJS, 173, 607
- Rich, R.M., et al. 2005, ApJ, 619, L107
- Schlegel, D.J., Finkbeiner, D.P. & Davis, M. 1998, ApJ, 500, 525
- Stern, D., et al. 2007, ApJ, 663, 677
- de Vries, W.H., et al. 2002, AJ, 123, 1784

Table 1. GALEX DIS Pointings Overlapping the Boötes Field

Field Name	α_{J2000}	δ_{J2000}	FUV Exposure Time(s)	NUV Exposure Time(s)
NGPDWS_00	219.15544	+35.16978	89492	89492
NGPDWS_01	217.85994	+35.41043	9508	9508
NGPDWS_02	219.20967	+34.09978	5918	5918
NGPDWS_03	218.15230	+34.60758	—	8798
NGPDWS_04	216.54480	+35.45390	—	8473
NGPDWS_05	217.20325	+34.60071	—	5493
NGPDWS_06	217.29972	+33.64349	—	9667
NGPDWS_07	216.12801	+33.30057	—	9650
NGPDWS_08	216.56646	+32.26761	—	8841
NGPDWS_09	218.92129	+33.18095	—	5801
NGPDWS_10	220.23785	+34.75341	1107	1107
NGPDWS_11	220.40109	+33.71991	1606	1606
NGPDWS_12	218.29527	+33.92749	—	8346
NGPDWS_13	217.85889	+33.01259	—	5343
NGPDWS_14	219.41794	+32.39430	—	7703
NGPDWS_15	216.39855	+34.34794	—	8783

Note. — These exposure times are for the GR3 images. With the release of GR4, many of these fields now have deeper images available.

Table 2. Systematic Test Results

z	FUV				NUV			
	Mean	RMS	Bias	Bias RMS	Mean	RMS	Bias	Bias RMS
0.1	22.97	0.42	−0.06	0.05	22.18	0.26	−0.05	0.06
0.2	23.63	0.11	−0.01	0.04	23.32	0.08	0.00	0.03
0.3	24.53	0.06	−0.05	0.01	24.10	0.06	0.05	0.03
0.4	24.95	0.04	0.00	0.02	24.34	0.04	0.09	0.04
0.5	25.19	0.03	−0.01	0.01	24.37	0.04	0.15	0.02
0.6	25.56	0.01	0.05	0.02	24.59	0.03	0.08	0.02

Note. — The values of the RMS, Bias and Bias RMS listed here were generated using 250 bootstrapped sampling realizations. The bias is defined as $\Delta m = \langle m_{measured} - m_{predicted} \rangle$. Here RMS indicates the RMS scatter in bootstrapped sample mean.

Table 3. Extinction-Corrected Magnitudes

z	m_{FUV}		σ_{FUV}		FUV K-corr		m_{NUV}		σ_{NUV}		NUV K-corr		V	
	$\hat{e} \geq 0.87$	$\hat{e} \geq 0.925$	$\hat{e} \geq 0.87$	$\hat{e} \geq 0.925$	$\hat{e} \geq 0.87$	$\hat{e} \geq 0.925$	$\hat{e} \geq 0.87$	$\hat{e} \geq 0.925$	$\hat{e} \geq 0.87$	$\hat{e} \geq 0.925$	$\hat{e} \geq 0.87$	$\hat{e} \geq 0.925$	$\hat{e} \geq 0.87$	$\hat{e} \geq 0.925$
0.1	23.55	23.46	0.25	0.25	-0.03	-0.03	22.74	22.74	0.19	0.20	0.42	0.36	17.12	17.12
0.2	24.43	24.21	0.19	0.18	-0.05	-0.01	23.89	23.82	0.12	0.14	0.61	0.41	18.59	18.51
0.3	25.52	25.32	0.17	0.30	-0.07	-0.03	24.92	25.05	0.10	0.25	0.73	0.53	19.77	19.47
0.4	26.00	25.74	0.12	0.20	-0.12	-0.02	25.27	25.42	0.13	0.21	0.89	0.53	20.73	20.68
0.5	27.00	27.30	0.20	0.41	-0.07	0.10	25.60	25.96	0.14	0.24	1.03	0.67	21.85	21.86
0.6	27.03	26.69	0.23	0.23	0.12	0.32	25.60	25.59	0.18	0.20	1.05	0.76	22.43	22.31

Note. — The uncertainties in FUV and NUV magnitudes are determined using the dispersion about the mean of the bootstrapped magnitudes. K-corrections are computed using the routines of Assef et al. (2008) and the modified spectral templates of Assef et al. (in prep).

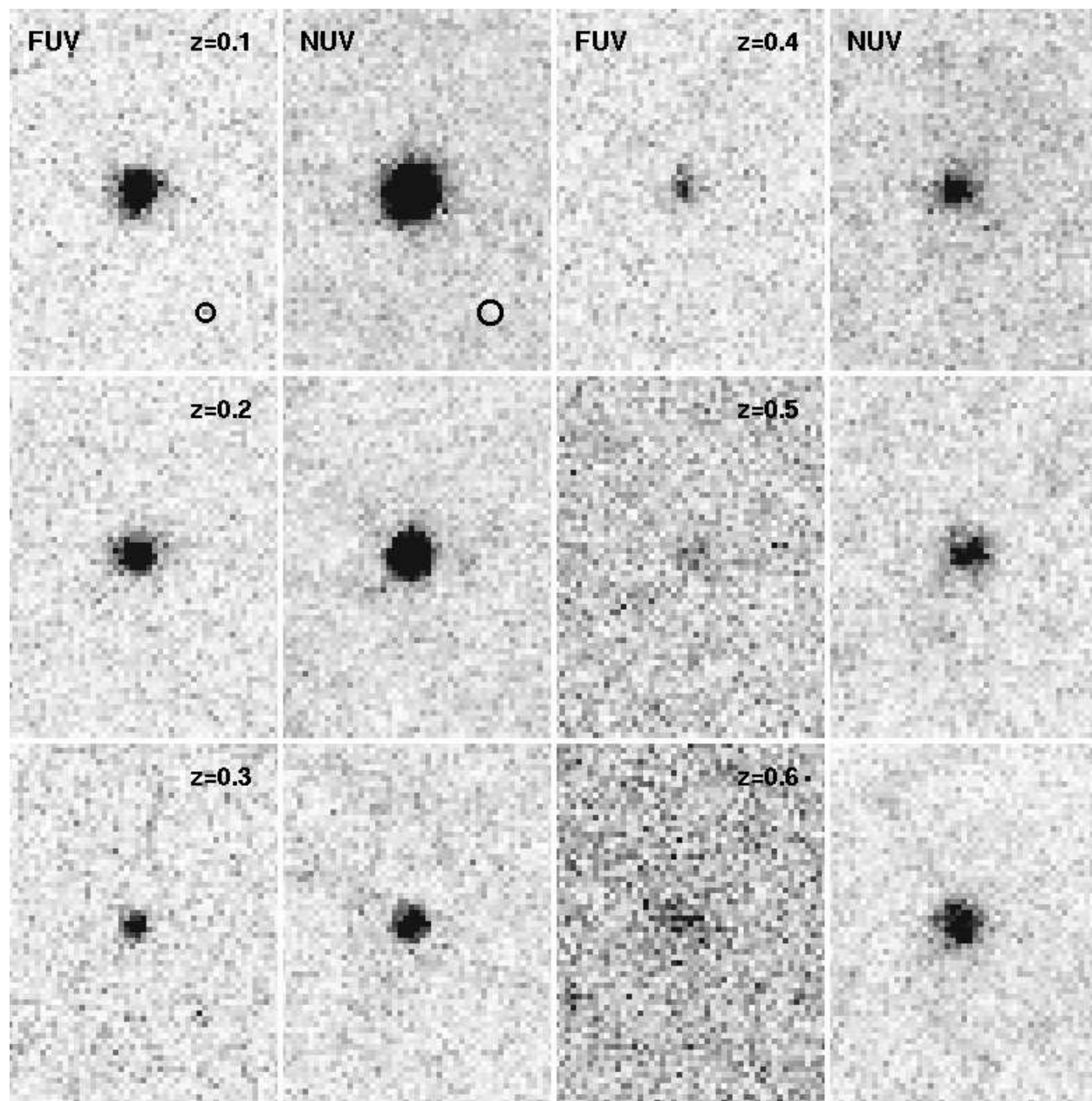


Fig. 1.— Stacked galaxy images. The first and third columns show the *FUV* images while second and fourth show the *NUV* images. The redshift increases first down columns and then across rows, as indicated. Each frame shows a region at the center of the stacked image that is approximately 45×65 pixels, where the plate scale is $1''.5$ per pixel. The *FUV* PSF FWHM of $4''.5$ and the *NUV* PSF FWHM of $6''.0$ are indicated by the circles in the $z = 0.1$ images. The images in the higher redshift bins appear to be extended due to jitter in the positions of the individual sample galaxies caused by finite pixel sizes.

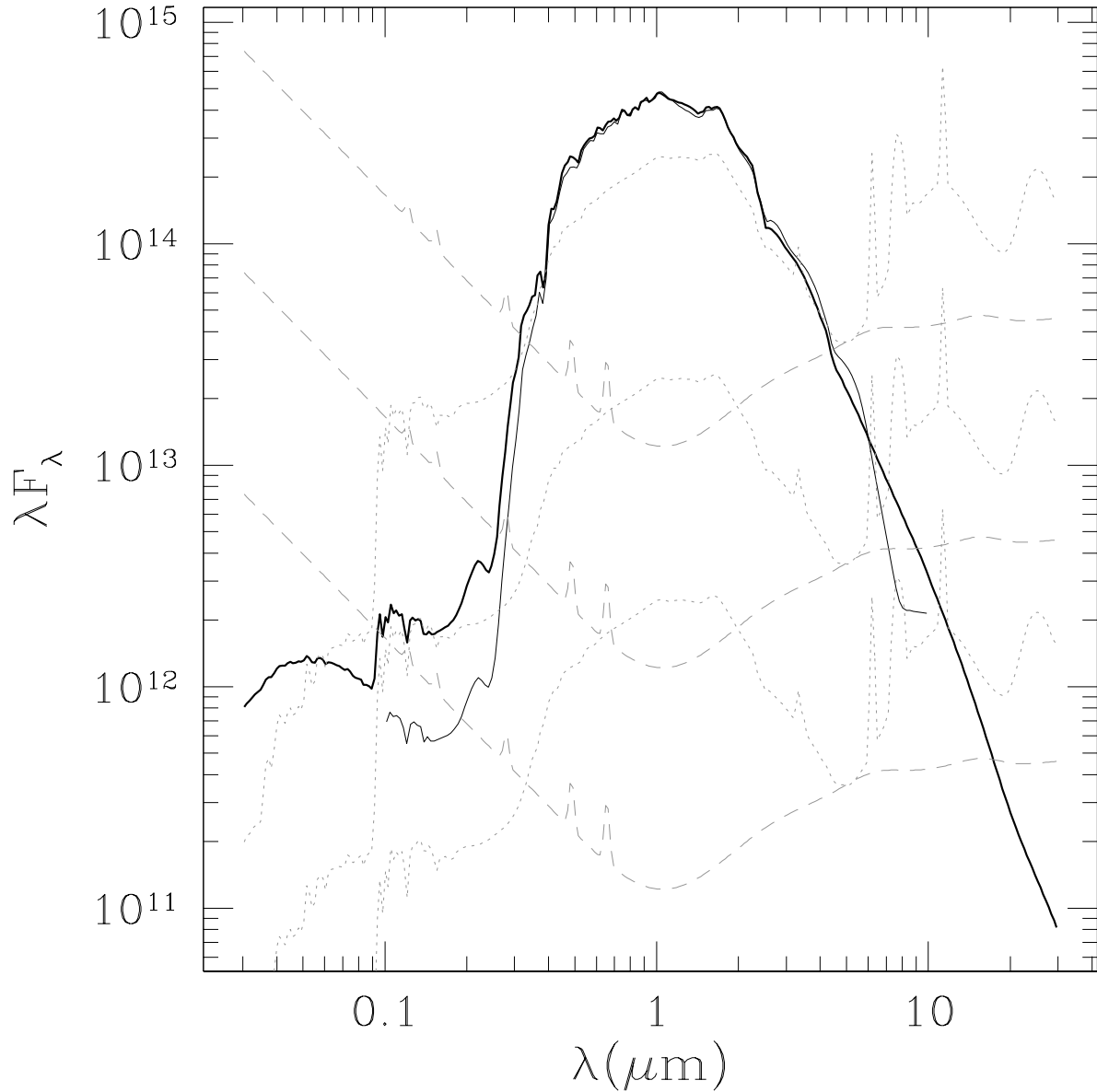


Fig. 2.— The elliptical template we use to compute K-corrections (*thick*), which has been modified from the original (*thin*) Assef et al. (2008) elliptical template, in internal template (arbitrary) units. Also shown are the AGN (*dashed*) and Sbc (*dotted*) templates, normalized to contain 1%, 10% and 100% of the bolometric luminosity contained in the elliptical template.

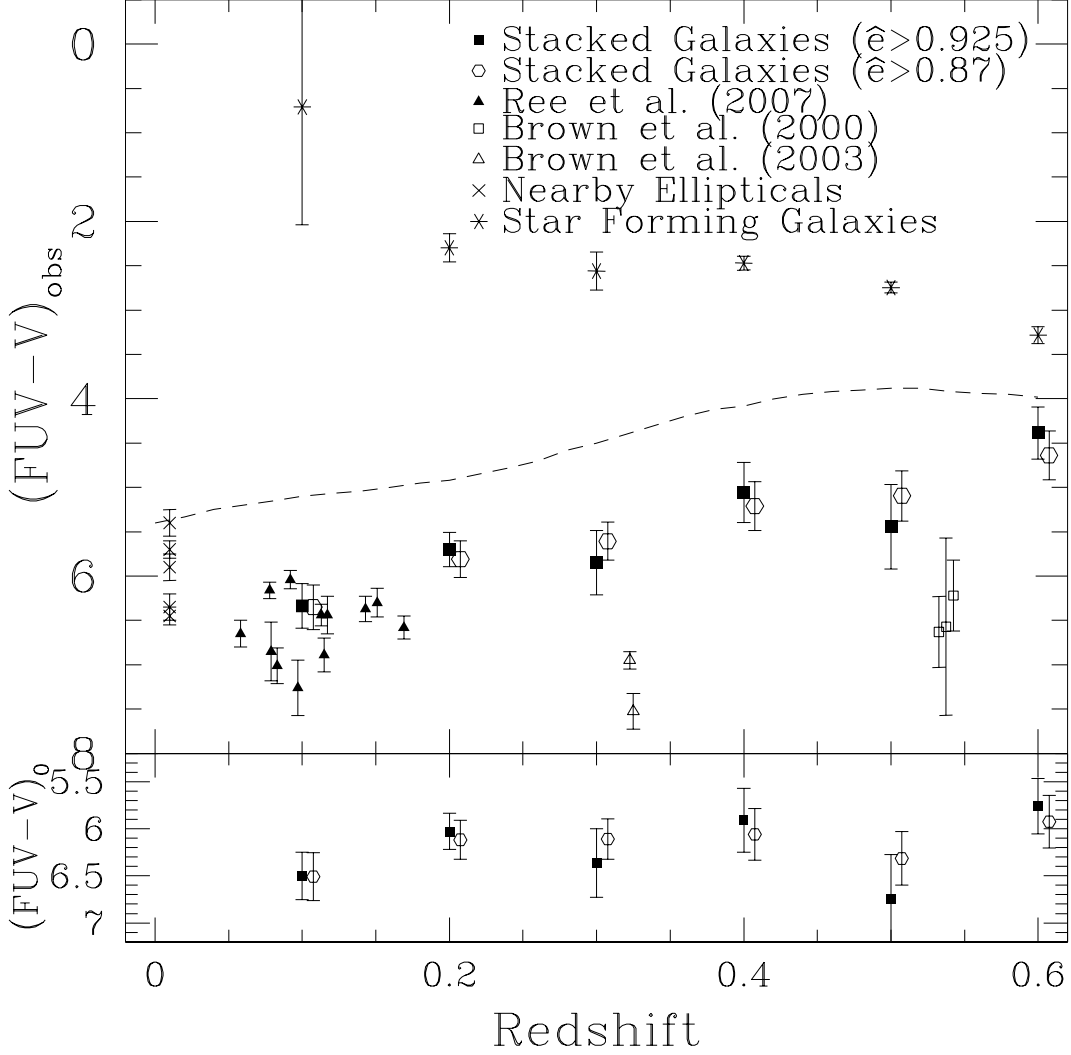


Fig. 3.— Evolution of the observed UV-optical colors of the stacked early-type galaxies ($\hat{e} \geq 0.925$), compared with the colors of galaxies presented in Ree et al. (2007). *Filled squares* and *open hexagons* indicate colors from our stacked galaxies, *open squares* from Brown et al. (2000), *open triangles* from Brown et al. (2003), *filled triangles* BCGs from Ree et al. (2007), *crosses* elliptical galaxies from the Fornax and Virgo clusters, and *stars* stacked star-forming galaxies. The *dashed line* shows the color that would be measured from NGC 1399 as a function of redshift. The lower panel shows colors K-corrected to redshift zero. The error on the FUV magnitudes is determined using the dispersion about the average bootstrapped FUV magnitude. Error bars show 1σ uncertainties.

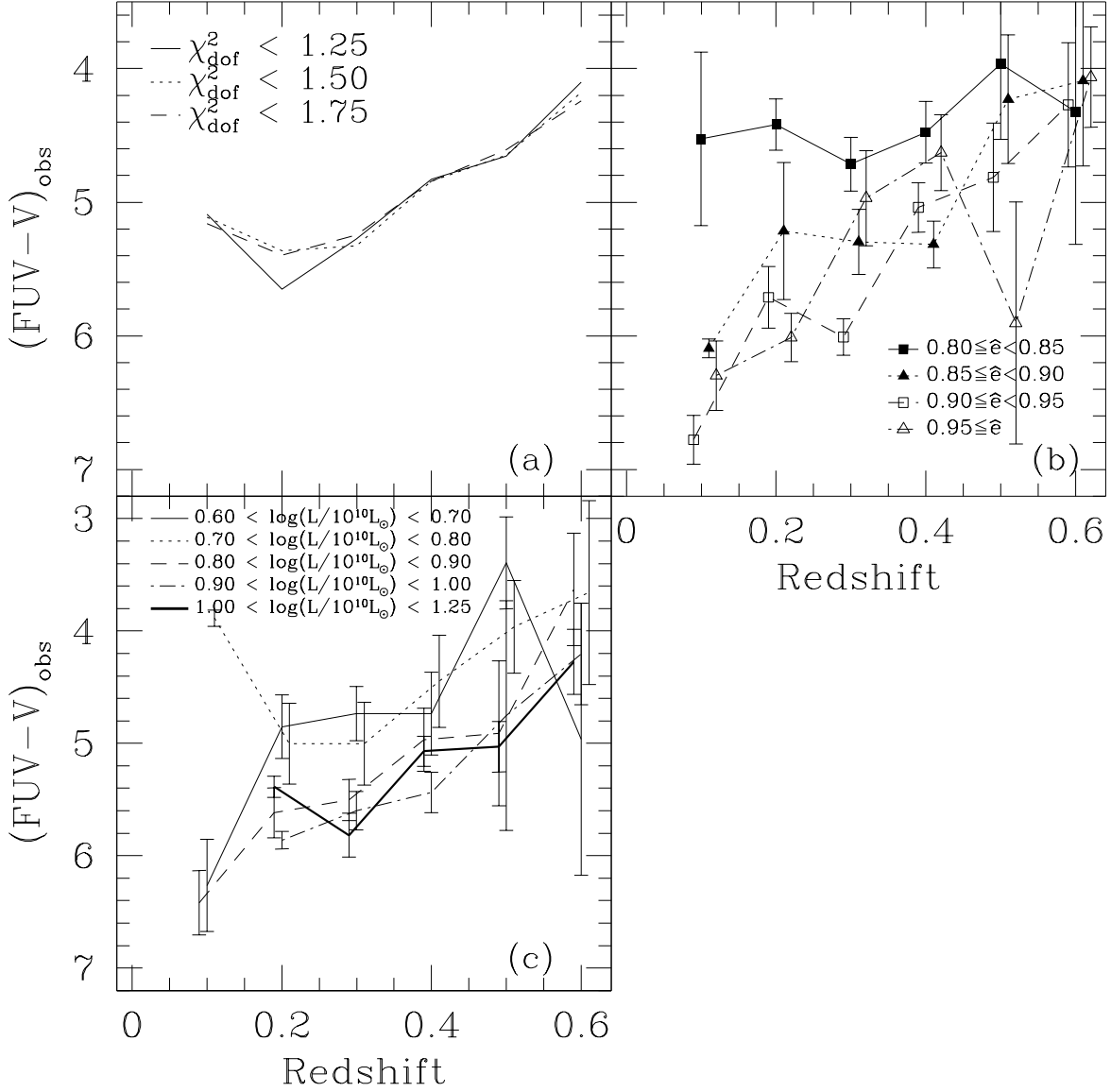


Fig. 4.— Dependence of the redshift evolution of the stacked galaxy color on the (a) goodness of SED fit, (b) elliptical fraction and (c) bolometric luminosity. The bolometric luminosity is determined by integrating the galaxy templates. It is clear that the trend shown in Fig. 3 is largely independent of the selection criteria. A trend toward redder $FUV - V$ with higher luminosity is apparent. Truncated lines in Figs. (b) and (c) are due to a lack of galaxies in the missing redshift bins.

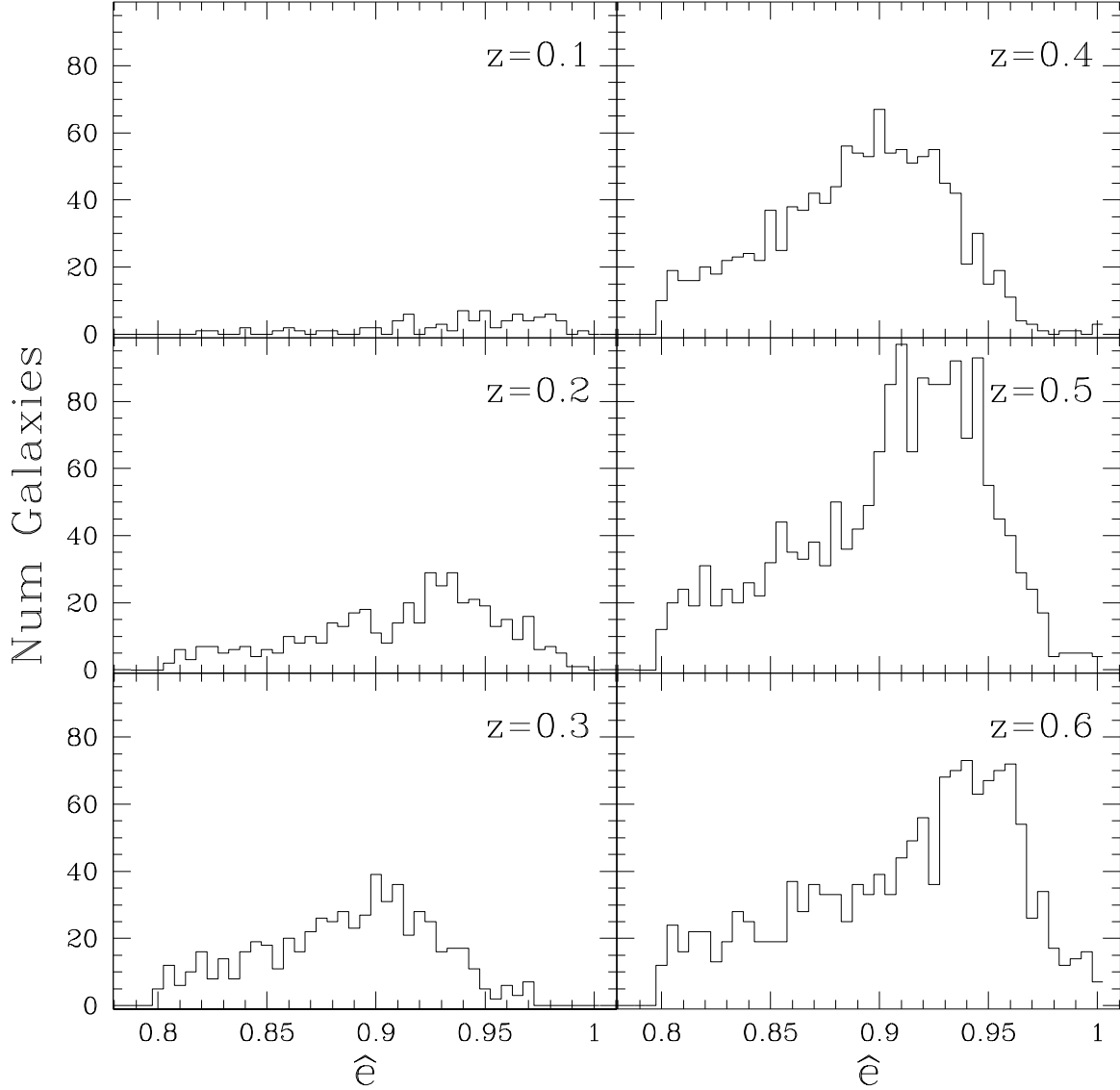


Fig. 5.— The distributions of the \hat{e} parameter in our different redshift bins for the initial galaxy sample ($\hat{e} > 0.80$). The fraction of blue (low \hat{e}) galaxies increases slowly with redshift, indicating an increase in fraction of young stars out to $z = 0.5$. In the $z = 0.5$ and $z = 0.6$ redshift bins, the IRAC bands are no longer sensitive to PAH emission from star-forming galaxies, and we see an increased fraction of sample galaxies at moderate to high \hat{e} .

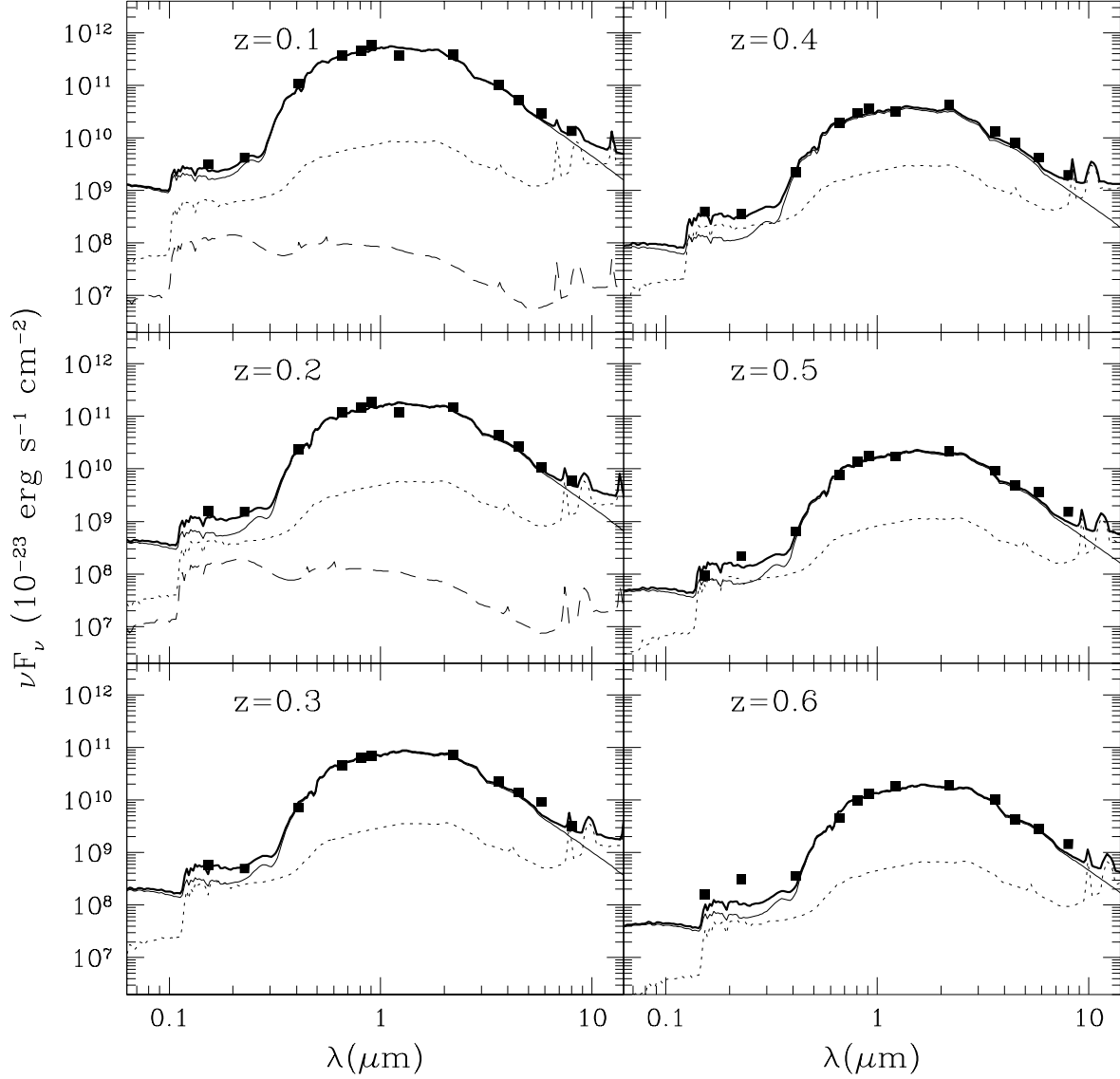


Fig. 6.— Fluxes and model SEDs for stacked galaxies from the $\hat{e} > 0.925$ sample in all redshift bins. The *dotted* line indicates the spiral component, the *dashed* line the irregular component and the *thin* line the elliptical component of the model spectra. The *heavy* line is the sum of the three components, and it is used to compute model magnitudes and K-corrections.

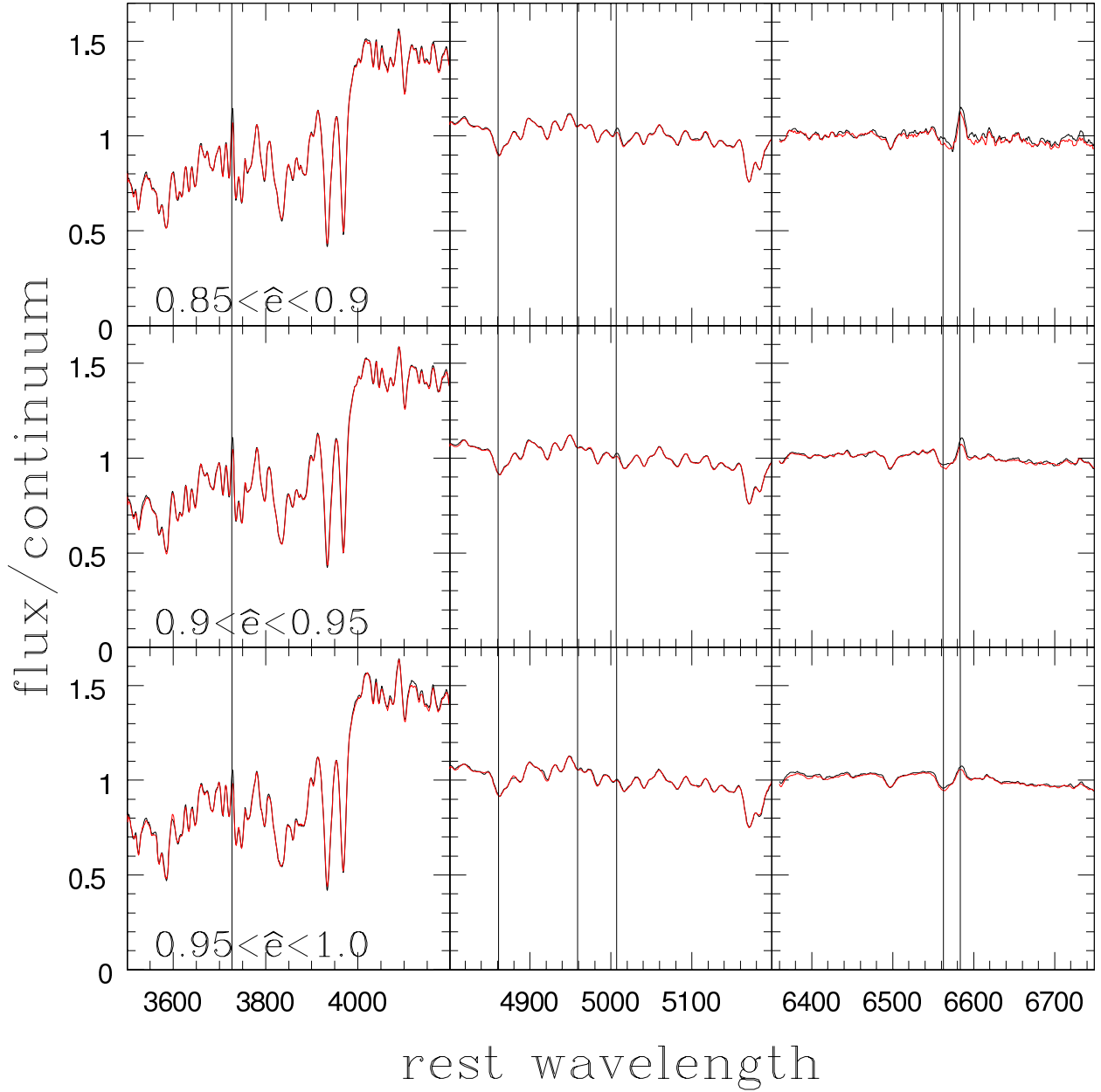


Fig. 7.— Stacked spectra centered near the [OII] (3727Å; *left*), [OIII] (5007Å; *middle*) and H α /[NII] (6563Å/6583Å; *right*) emission lines. Both the mean (*gray*) and median (*red*) spectra are shown. The constituent galaxies were taken from the $\hat{e} > 0.85$ sample and divided into \hat{e} bins as shown. The spectra have been normalized so the average value across the displayed range is 1. Vertical lines indicate important emission lines.

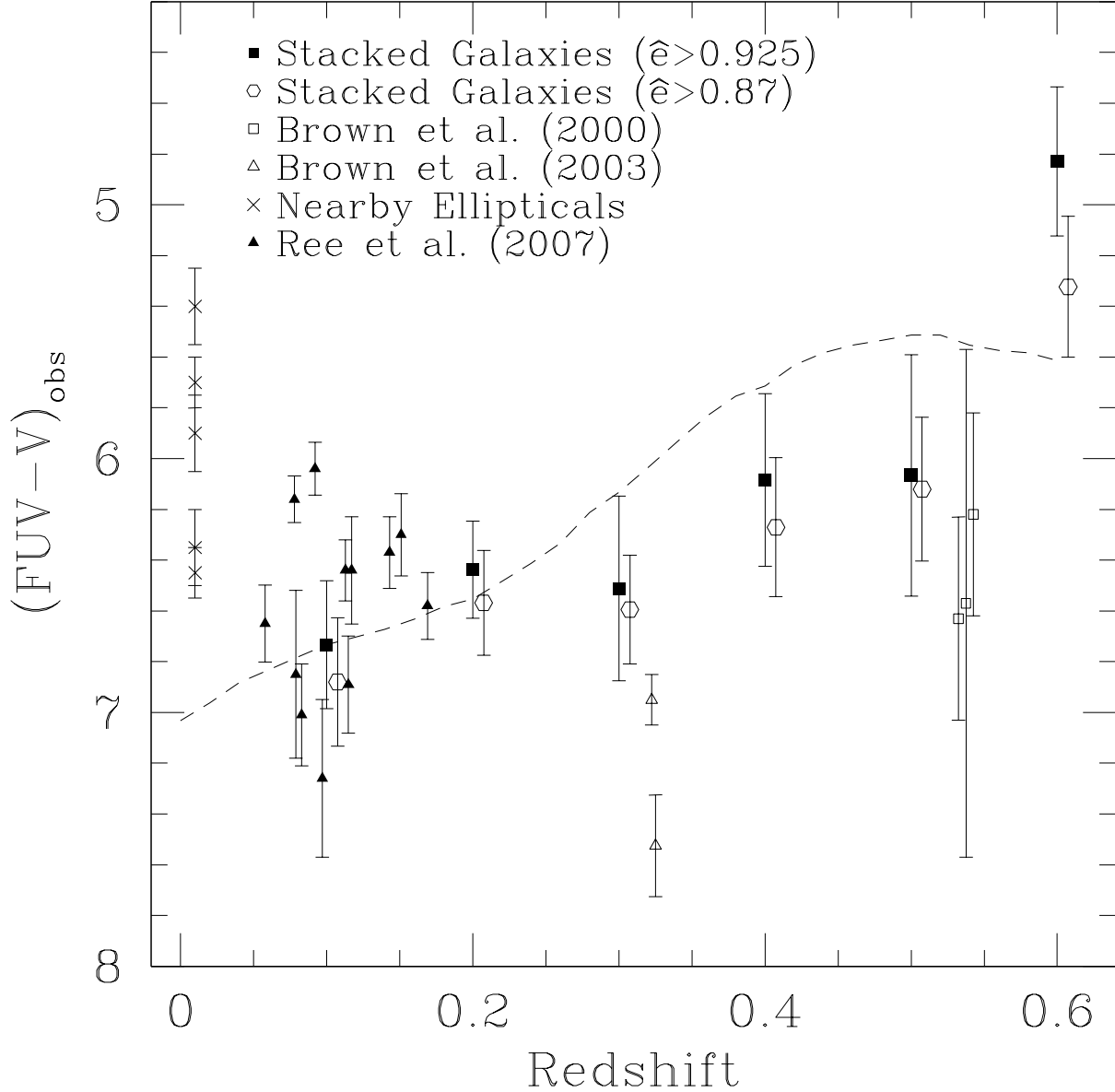


Fig. 8.— Evolution of the observed colors of the stacked elliptical galaxies, corrected for star formation. Flux contributed by young stars has been subtracted using the method described in Eq. (5). The unevolving colors (*dashed line*) from Fig. 3 have been translated to pass through the $z = 0.1$ point, but have not been otherwise modified. All other symbols are the same as in Fig. 3. Assuming Gaussian errors, the $\hat{e} > 0.87$ colors at $z \leq 0.5$ are inconsistent with the non-evolving “model” at $> 99\%$ confidence.

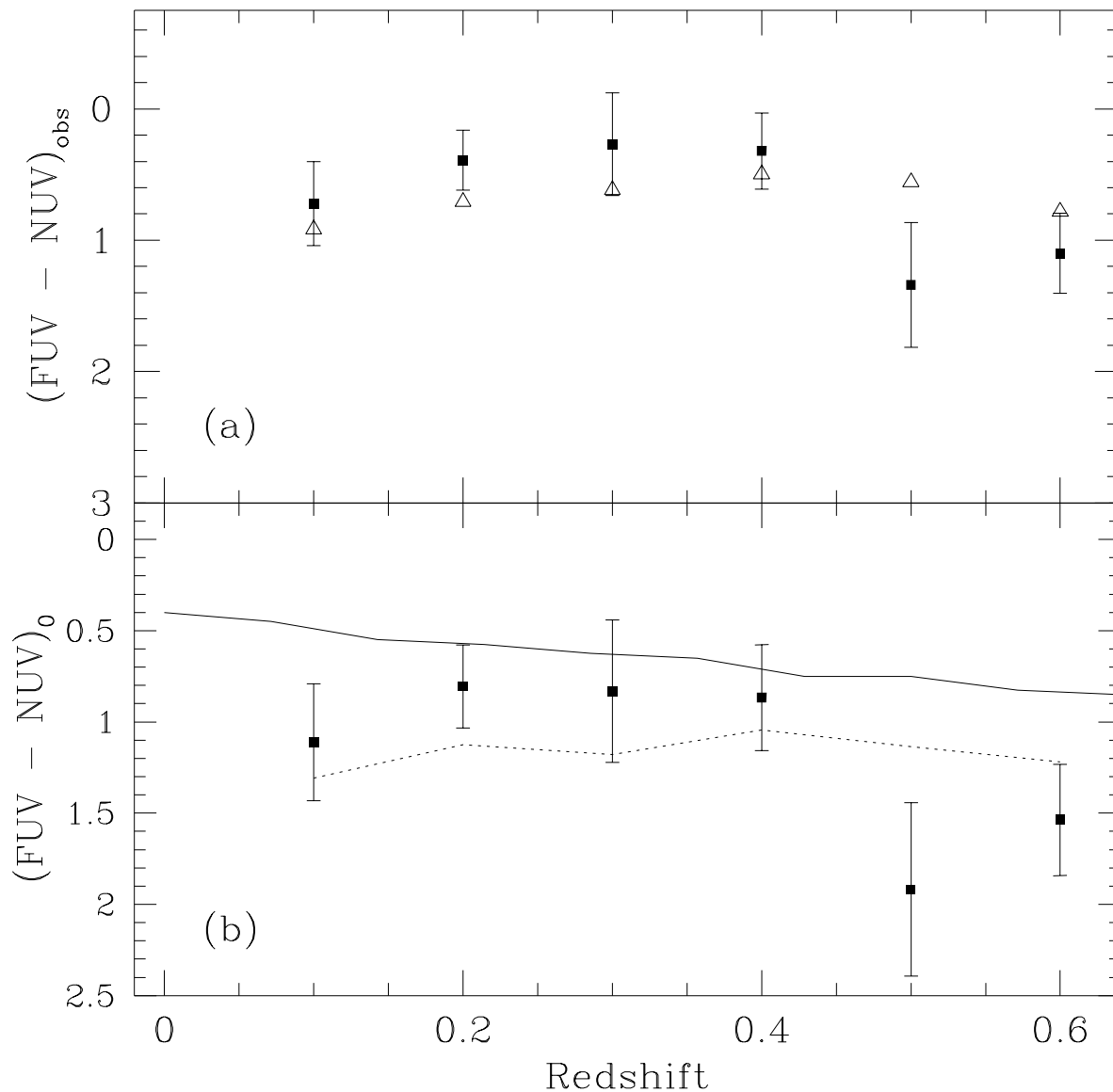


Fig. 9.— Evolution of the UV color, uncorrected for star formation. Panel (a) shows the observer frame evolution of UV color. The *filled squares* give the UV colors of the stacked galaxies, and the *open triangles* give the colors predicted by the model spectra. Panel (b) shows the rest frame evolution of UV color, with error bars from the measured fluxes only. The *solid line* shows the evolution predicted by the model of Han, Podsiadlowski & Lynas-Gray (2007), and the *dashed line* shows the colors of the model galaxy spectra.

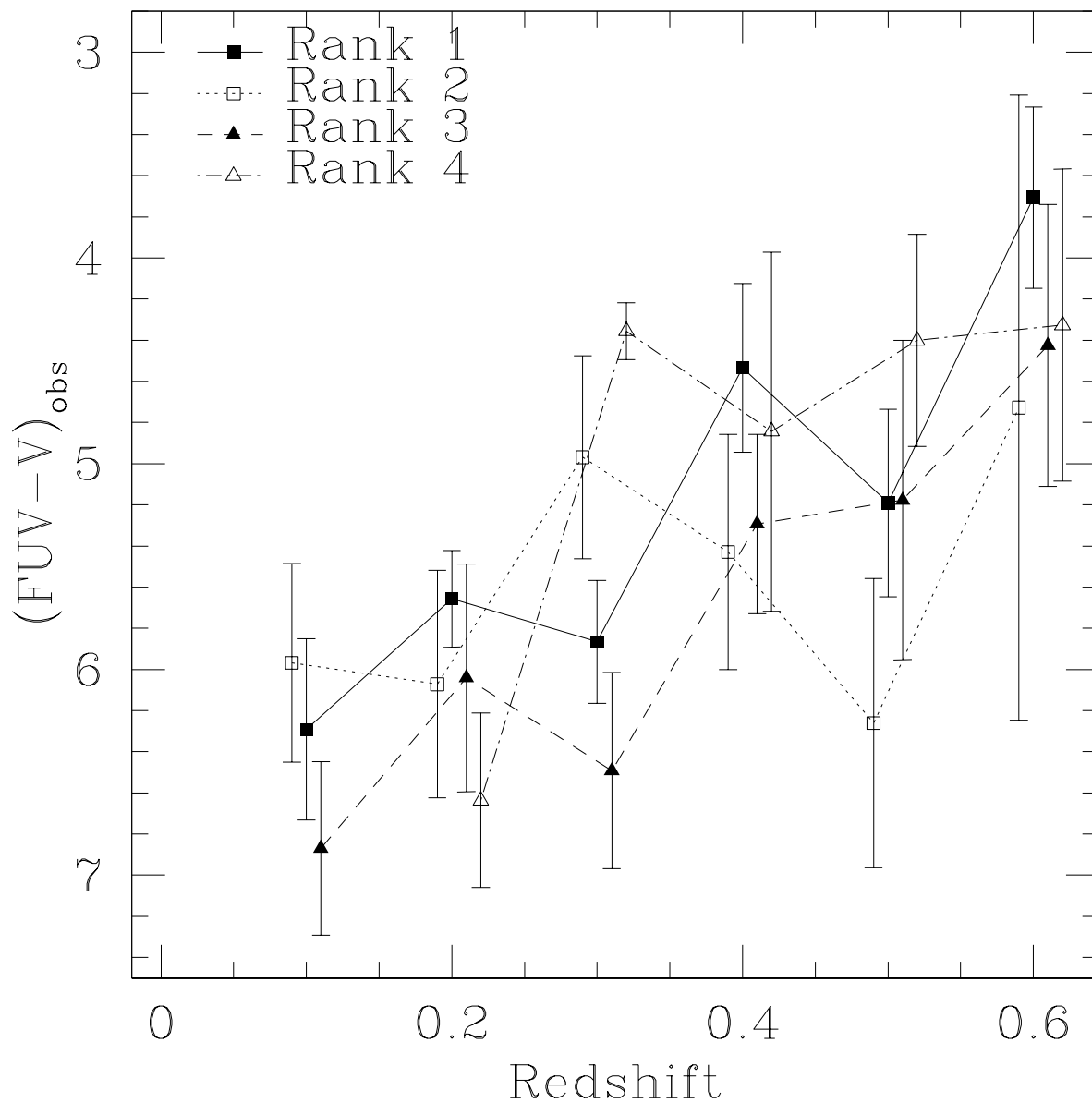


Fig. 10.— Dependence of $FUV - V$ on galaxy environment. Rank 1 galaxies (*filled squares*) fall in the least dense regions while Rank 4 galaxies (*open triangles*) fall in the densest regions. The data show no significant pattern, indicating that either a galaxy’s environment has little impact on its UV properties or the influence of environment is limited to so few galaxies that the other galaxies in the bin overwhelm any effect.